HHS Public Access

Author manuscript

J Memb Sci. Author manuscript; available in PMC 2020 January 15.

Published in final edited form as:

J Memb Sci. 2020 January 15; 594: . doi:10.1016/j.memsci.2019.117454.

Pd/Fe nanoparticle integrated PMAA-PVDF membranes for chloro-organic remediation from synthetic and site groundwater

Hongyi Wan[a], **Md Saiful Islam**[a], **Nicolas J. Briot**[a], **Matthew Schnobrich**[c], **Lucy Pacholik**[b], **Lindell Ormsbee**[b], **Dibakar Bhattacharyya**[a,*]

[a]Department of Chemical and Materials Engineering, University of Kentucky, Lexington, KY, 40506-0046, USA

[b]Department of Civil Engineering University of Kentucky, Lexington, KY, 40506-0046, USA

[c]Arcadis, Lexington, KY, 40509, USA

Abstract

The poly(methacrylic acid) (PMAA) was synthesized in the pores of commercial microfiltration PVDF membranes to allow incorporation of catalytic palladium/iron (Pd/Fe) nanoparticles for groundwater remediation. Particles of 17.1 ± 4.9 nm size were observed throughout the pores of membranes using a focused ion beam. To understand the role of Pd fractions and particle compositions, 2-chlorobiphenyl was used as a model compound in solution phase studies. Results show H_2 production (Fe^0 corrosion in water) is a function of Pd coverage on the Fe. Insufficient H_2 production caused by higher coverage (> 10.4% for 5.5 wt%) hindered dechlorination rate. With 0.5 wt% Pd, palladized-Fe reaction rate (surface area normalized reaction rate, k_{sa} = 0.12 L/(m^2-h) was considerably higher than isolated Pd and Fe particles. For groundwater, in a single pass of Pd/Fe-PMAA-PVDF membranes (0.5 wt% Pd), chlorinated organics, such as trichloroethylene (177 ppb) and carbon tetrachloride (35 ppb), were degraded to 16 and 0.3 ppb, respectively, at 2.2 seconds of residence time. The degradation rate (observed k_{sa}) followed the order of carbon tetrachloride > trichloroethylene > tetrachloroethylene > chloroform. A 36 h continuous flow study with organic mixture and the regeneration process show the potential for on-site remediation.

Keywords

Pd/Fe membrane reactor; Groundwater remediation; Chloro-organics removal; Focused ion beam; H_2 production

*Corresponding author. Chemical and Materials Engineering, 177 FPAT Bldg, University of Kentucky, Lexington, KY, 40506, USA. db@uky.edu (D. Bhattacharyya).

Conflicts of interest

The authors declare no conflict of interest.

Appendix A. Supplementary data

Supplementary data to this article can be found online at https://doi.org/10.1016/j.memsci.2019.117454.

1. Introduction

Membrane technologies have been widely studied and applied in various separation processes over the past decade [1-7]. Besides the advances in separation, the incorporation of metals, non-metallic inorganic substances and enzymes into membrane systems have provided catalytic functions and allowed for applications in chemical synthesis and water treatment as well as a reduction in membrane fouling [8-14]. In water treatment, catalytic membranes show great potential in the remediation of contaminated water by oxidation or reduction methods [15-17]. They also provide an effective treatment technology with a small footprint and low energy cost [18].

Specific to toxic chlorinated aliphatic/aromatic hydrocarbons, trichloroethylene (TCE) and polychlorinated biphenyls (PCBs) are two of the contaminants of most concern [19-22]. Reductive dechlorination of TCE, PCBs and other toxic chlorinated hydrocarbons has been investigated using palladium/iron (Pd/Fe) bimetallic nanoparticles [23-27]. Field scale injection of stabilized Pd/Fe or Fe nanoparticles (around 15–200 nm) were also studied [28-30]. However, issues concerned with such nanoscale Pd/Fe or Fe applications include particle agglomeration, limited subsurface mobility, aging, oxidation, leaching and potential secondary environmental risks. Such problems could hinder the long-term application and wide usage of these techniques [31-36].

The integration of nanoparticles and polymeric membranes could address some of these issues because of the large surface area, stability and the potential for versatile functionalities of membrane domains [37,38]. Among the integration methods (which include sol-gel process, particle deposition, in situ reduction, ion-exchange and in situ polymer reaction [39-43]), ion-exchange using carboxyl groups (-COOH) has been shown to effectively capture metal ions, which shows the potential to prevent the leaching of incorporated nanoparticles [44-46].

The synthesis of poly(acrylic acid) (PAA)-polyvinylidene fluoride (PVDF) membranes along with novel ion-exchange processes for Pd/Fe particle incorporation have been reported for the treatment of chlorinated organic compounds [38,47-49]. To scale up the synthesis of catalytic membranes, additional process optimizations and advanced material characterizations need to be performed. Although acrylic acid (vapor pressure: 400 Pa at 20 °C) is used in many industries, methacrylic acid (MAA), an alternative with similar chemical structure and less volatile nature (vapor pressure: 93 Pa at 20 °C), was used as a monomer in this study to introduce carboxyl groups in commercial PVDF membranes. In addition, due to the highly porous structure and non-conductive nature of polymeric membrane membranes, the characterization of incorporated particles, using a scanning electron microscope (SEM), is usually limited on the external surface of membranes. This limitation impedes the understanding of the intrinsic properties of these particles inside the pores, such as reactivity and hydrophilicity [50,51]. In our previous work, particles underneath the membrane surface were observed by lifting a lamella (~20 μm thick) of membrane surface using focused ion beam (FIB) [52]. Limited by the dimensions of lamella, this well-developed FIB lamella method [53,54] is not able to make a sample for the characterization on the entire set of membrane pores. In this study, FIB was used to precisely

slice an entire cross-section of each membrane. Particle size and density were then quantified through the entire depth of the membrane pores. The results were then used in a plug-flow model analysis of groundwater remediation.

For remediation, both nanoparticle aspects (the role of Pd, particle composition and corresponding H_2 production) and various water conditions (pH and temperature) were investigated by using 2-chlorobiphenyl (PCB 1) as a model compound. The PCB 1, one of the toxic PCBs, has recalcitrant nature and it can be directly dechlorinated to biphenyl without any intermediates [55]. The Pd/Fe dechlorination method relies on the activation of H_2 by Pd. The H_2 is yielded from Fe^0 (metallic Fe) corrosion with water, and the produced H_2 is then activated by Pd to form highly reactive atomic hydrogen for hydrodechlorination [27,56]. Studies show a positive correlation between the content of Pd on the Pd/Fe bimetallic nanoparticles (0.1–1.0 wt% of Fe) and the resulting dechlorination rate [57,58]. However, the effects of Pd surface coverage on H_2 production and corresponding dechlorination performance have not been well investigated.

In this study, the investigation of nanoparticles intrinsic properties with model compound PCB 1 guided the application of the Pd/Fe nanoparticles incorporated poly(methacrylic acid) (PMAA) - PVDF membranes in the treatment of contaminated groundwater. The groundwater samples were collected from an industrial site and the groundwater contains a mixture of chlorinated aliphatic hydrocarbons, such as TCE and carbon tetrachloride (in 10–1000 ppb range). The objectives of this research are: **(1)** Introduction of carboxyl groups in the pores of commercial PVDF membranes in a water-based system using a less volatile monomer – methacrylic acid; **(2)** Quantification of the size and distributions of incorporated Pd/Fe nanoparticles across the entire membrane pores, using a FIB technique, for use in subsequent reactivity analysis; **(3)** Investigation the Pd fraction loadings and particle compositions (palladized-Fe versus isolated Pd and Fe) by quantifying H_2 production and corresponding dechlorination performance; **(4)** Effective remediation of the collected contaminated groundwater samples using the Pd/Fe functionalized membranes and comparing the degradation rates between individual contaminants and finally, **(5)** Long-term study (36 h continuous flow) were performed to evaluate the stability and regeneration of reactive particles, as well as to establish the potential for on-site application.

2. Materials and methods

2.1. Materials

The following chemicals were used as received: sodium hydroxide (1 M), sulfuric acid (0.5 M), hexanes (> 99%), anhydrous sodium sulfate and ferrous sulfate were obtained from Fisher Scientific. Sodium borohydride (99.99%), sodium carboxymethyl cellulose (M_w~90k), potassium tetrachloropalladate (II) (98%), biphenyl_d_{10} (99 atom % D), trichloroethylene (99.5%) and tetrachloroethylene (> 99%) were purchased from Sigma-Aldrich. PVDF powder was purchased from Polysciences, Inc. Potassium persulfate (98%), N,N′-methylenebisacrylamide (NNMA, 99%) and methacrylic acid (99.5%, stabilized) were received from Acros Organics. Nitric Acid (AR select ACS) was ordered from Macron Fine Chemicals. 2-chlorobiphenyl (> 97%) and its analytical solution (100 ppm in hexane) as well as the analytical standards of chloroform (100 ppm in methanol), carbon tetrachloride

(100 ppm in methanol) and hexachlorobutadiene (100 ppm in methanol) were obtained from Ultra Scientific. Ethanol (200 proof) was bought from EMD Millipore Corporation. Full scale PVDF 700 microfiltration membranes were obtained from Solecta, Inc. DVPP04700 membranes were purchased from Millipore. Deoxygenated water was obtained by purging N_2 into deionized ultra-filtered (DIUF) water for 30 min.

2.2. Synthesis of palladium/iron nanoparticles in solution phase

The palladized-Fe bimetallic and isolated Pd and Fe nanoparticles were synthesized with sodium carboxymethylcellulose (CMC) as a stabilizer. The synthesis method was modified based on the literature [56]. The details are illustrated in SI section 1.

2.3. Synthesis of palladium/iron nanoparticle incorporated PMAA-PVDF membranes

The Pd/Fe nanoparticles were synthesized in situ within the pores of functionalized membranes by ion-exchange and reduction reaction processes (Fig. 1). The membrane functionalization method was modified based on our previous work [49] and the details are mentioned in SI section 2. In this study, methacrylic acid was used as an alternative to acrylic acid. Instead of immersing the membranes at different solutions, the ion-exchange and subsequent nanoparticles synthesis were conducted by permeating the Na^+, Fe^{2+} and NaOH solutions through the membrane without dismantling the membrane filtration set up. This modified method has a potential to be applied to commercial spiral wound and hollow fiber membrane modules.

2.4. Characterization

2.4.1. Membrane surface morphology—The morphology of the membrane surface and the size of the pores were observed using SEM and counted using ImageJ software. The membrane hydrophilicity was tested using a drop shape analyzer (DSA 100, Krüss). Attenuated total reflectance-Fourier transform infrared spectroscopy (ATR-FTIR, Varian 7000e) was used to identify the successful functionalization of the PMAA.

2.4.2. Size, composition and distribution of Pd/Fe bimetallic particles inside membrane pores—Particle size and distribution were determined across the entire depth of membranes by directly imaging the cross-section plane of the membrane in the SEM. To maintain the structures of particles and membrane pores, an advanced cross-sectioning method using focused ion beam (FIB, FEI Helios Nanolab 660) was developed. A cross-sectional plane was first created by fracturing a small piece of the membrane following immersion in liquid nitrogen. The FIB was then performed to expose an undamaged region of the membrane. For gallium ion-based FIB systems, typical cross-sectioning processes only expose the first few tens of micrometers below the surface [52,59]. The advanced FIB preparation method allows exposure of the entire membrane cross-section (170 μm), creating a flat and smooth surface suitable for SEM imaging and elemental analysis using energy dispersive x-ray spectroscopy (EDS, Oxford Instruments X-Max^N 80 detector). The details of FIB preparation are described in SI section 3. Particle composition was also analyzed using X-ray diffractometer (Siemens D500, Cu Kα 1.5418 Å).

2.5. Analytical methods

The details of analytical methods, such as gas chromatography–mass spectrometry (GC-MS), chloride electrode and inductively coupled plasma optical emission spectroscopy (ICP-OES), are summarized in SI section 4. The measurement of hydrogen production is described in SI section 5.

2.6. Dechlorination study in solution phase

The details of the solution phase studies for model compound PCB 1 and for the collected groundwater samples are summarized in SI section 6.

2.7. Dechlorination in the membrane domain convective flow study

Pd/Fe functionalized membranes, with an effective external area of 11.2 cm^2, were evaluated using a dead-end filtration cell (HP4750 stirred cell, STERLITECH corp.). The residence time (the average time particles spent in the membrane) was controlled by changing the operating pressure. In this study, the groundwater samples were permeated through the Pd/Fe incorporated membranes at various operation pressures (0.34, 0.69 and 1.0 bar). The functionalized membranes without Pd/Fe particles were also investigated as a control group to determine the loss of target chlorinated organics due to adsorption and evaporation.

3. Results and discussion

3.1. Membrane functionalization and characterization

3.1.1. Properties of functionalized membranes—The membrane functionalization includes PMAA polymerization and nanoparticles incorporation (Fig. 1). The successful polymerization of PMAA (validated by ATR-FTIR analysis in SI section 7) changed the properties of the pre-hydrophilized commercial PVDF membranes (Solecta, Inc.) (Table 1). Due to the ionization of the carboxyl group, the PMAA chains swell when the solution pH > pKa of PMAA, which was reported as 4.6–4.8 [60]. A greater pH (> pKa) was found to decrease the membrane pore size and permeability, and vice versa. The permeability ($Lm^{-2}h^{-1}bar^{-1}$, LMH/bar) was measured as 543 ± 4, 86.3 ± 3.6 and 18.2 ± 0.5 at pH 2.3, pH 5.5 and pH 10.5, respectively (Fig. 2). The permeability at pH 2.3 was measured at 0.34, 0.69 and 1.03 bar and the permeability at pH 5.5 and pH 10.5 were measured at 1.72, 3.45 and 5.17 bar. A reversible permeability at different pH was also observed. The permeability decreased with an increase of pH and recovered after the pH adjusted back to the lower value.

This pH responsive behavior was also observed during the measurement of contact angle (Fig. 3). The membrane pieces were immersed at different pH and then dried under a nitrogen flow before the measurement. The results show that contact angle measured at pH 2.3 (68.3 ± 2.7) is greater than the measurement at pH 10.5 (48.2 ± 1.2), which means the membrane surface is more hydrophilic at pH 10.5. Furthermore, the water droplets at pH 10.5 wetted the surface more rapidly and spread out over 300 s. Cheng et al. reported a similar pH responsive wettability on an electrospun PVDF-poly(acrylic acid) nanofiber membrane [61]. The ionization of carboxyl group stretched out the polymer chain and promoted the replacement of air trapped in the pores by water, which accelerated the surface

wetting. Such a pH responsive behavior on permeability and wettability could be applied in selectively separation and drug release [62-64].

To immobilize metal nanoparticles, the functionalized PMAA-PVDF membranes undergo two steps of ion-exchange (Na^+ and Fe^{2+}) and reduction of Fe^{2+}. Since the pH was changed during these steps, the membrane permeability also changed (Fig. S.5). The permeability of synthesized Pd/Fe-PMAA-PVDF membrane was measured as 44.2 ± 0.8 LMH/bar at pH 5.5. As shown in Fig. 2, the incorporation of particles decreases the permeability and compromises the pH responsive behavior. From pH 5.5 to pH 10.5, the permeability decreased 3.8-fold for the PMAA-PVDF membrane but only decreased 1.1-fold when embedded with nanoparticles. No permeability test was conducted at pH 2.3, since the incorporated Fe particles would be easily dissolved.

3.1.2. Size and distribution of particles throughout the membrane pores—The size and distribution of catalytic particles have significant impacts on dechlorination performance, especially for those particles in the pores of membrane. The characterization of those particles inside membrane pores could be achieved by using a developed FIB cross-sectioning method. The FIB could precisely slice a smooth cross-section plane and maintain the pore structures. To present the FIB-SEM technique, the Millipore PVDF membrane (thickness: 80 μm) was used only for characterization due to its more porous structures and its lack of any supporting materials. As shown in Fig. 4a, the FIB-modified area, in the center of the cross-section plane, is smoother and clearer than the unmodified area. As summarized in Fig. 4d, the particle size was uniform inside membrane pores (23.2 ± 8.2 nm) but smaller than those nanoparticles (39.1 ± 9.3 nm) located on the top and bottom surfaces. The size difference was caused by the formation of PMAA rich layer (thickness: ~2 μm), which was not restrained by the PVDF pores, on the top and bottom surfaces of the membrane. The particle distribution was observed using EDS mapping. Since the fluorine to carbon ratio is constant in every repeat unit of the PVDF (F/C = 1/1), the iron to fluorine ratio is used to determine the particle distribution inside the membrane pores. A higher distribution of particles on top and bottom surface of the membrane was also observed.

The characterization of functionalized Solecta PVDF 700 membranes, which have a backing material and were applied in the groundwater study, was also conducted (SI section 8). The EDS mapping, in Fig. S.6d, shows that the Fe was mainly observed at the top PVDF layer (43 μm) and insignificant Fe distribution was found in the backing material (127 μm). A greater Fe density and relatively large particles (20.2 ± 6.6 nm) were also observed on both top and bottom surfaces of the PVDF layer. A uniform size and density distribution of particles (17.1 ± 4.9 nm) were found inside the PVDF layer (Fig. S.6e). Since the Pd loading is only a trace fraction in the membranes (0.5 wt% of Fe, 0.0125 wt% of the membranes), the membrane domain had a strong background noise in the Pd analysis of individual Pd/Fe nanoparticles under SEM with EDS detector. To improve the accuracy of element analysis on the individual nanoparticles, the nanoparticles were synthesized without membrane domains and then characterized in TEM (in section 3.2.1).

3.2. Evaluation of the reactivity of Pd/Fe nanoparticles through the dechlorination studies in solution phase

In this section, the PCB 1 (a model compound) dechlorination experiments were conducted in solution phase, without membrane domain, to understand the intrinsic properties of Pd/Fe particles. Based on the material characterization of the Pd crystalline pattern (XRD) and the size of the nanoparticles (TEM), a theoretical surface coverage of a Pd monolayer on Fe particles was calculated. The surface coverage was used to find the optimal Pd fractions on Fe by measuring H_2 production and overall dechlorination performance. The composition of particles, that is palladized-Fe or isolated Pd and Fe nanoparticles, were also studied. In addition, the solution phase studies were conducted at same pH condition of the collected groundwater samples (pH 7.8) as well as at different pH and temperature conditions (4–40 °C).

3.2.1. Effects of Pd fractions and Pd/Fe compositions in hydrogen production and dechlorination performance—The dechlorination of PCB 1 by Pd/Fe nanoparticles can be described as equations (1)-(4). As a catalyst, an increase of the amount of Pd should accelerate the dechlorination reaction under sufficient H_2 condition, such as Pd particles under a H_2 stream [65-67]. However, when the corrosion of Fe is the source for H_2, excess Pd coverage on Fe could reduce the exposed Fe for H_2 production, leading to a decrease in the dechlorination rate. In Fig. 5b, a tradeoff between increasing Pd fraction (analyzed using ICP, results shown in SI section 9) and H_2 production was observed for a same source of Fe. Tee et al. reported the study with Ni/Fe bimetallic particles and they also found a 10-fold decrease in H_2 generation with an increase of Ni content from 20% to 75% [68]. For ease of comparison, H_2 production was normalized to the batches with 0% Pd. Based on the GC analysis, nearly 51.2×10^{-7} mol hydrogen was produced by the 0 wt% Pd batches at 10 min interval (the details of the derivation are summarized in SI section 5). Stoichiometrically, the complete dechlorination of 1.1×10^{-7} mol PCB 1 to biphenyl requires 0.55×10^{-7} moL H_2. In results, 0.61×10^{-7} and 0.46×10^{-7} moL H_2 was produced at the 5.5 and 12 wt% Pd batches, respectively. Insufficient H_2 was produced at the 12 wt% Pd batches, leading to a less dechlorination compared to the batches with 5.5 wt% and even 0.5 wt% Pd.

The formation of Pd on the surface of Fe^0:

$$Fe^0 + PdCl_4^{2-} \rightarrow Pd + Fe^{2+} + 4Cl^- \quad (1)$$

The production of H_2 by the corrosion of Fe^0 in water [69]:

$$Fe^0 + 2H_2O \rightarrow Fe^{2+} + H_2\uparrow + 2OH^- \quad (2)$$

The formation of atomic hydrogen and the dechlorination of PCB 1 [58,70]:

$$H_2\uparrow \xrightarrow{Pd} 2H* \quad (3)$$

$$C_{12}H_9Cl\,(PCB\,1) + 2H\,* \rightarrow C_{12}H_{10}\,(biphenyl) + H^+ + Cl^- \quad (4)$$

For the formation of Pd/Fe nanoparticles, the Pd^{2+} ions were reduced by metallic Fe and a layer of Pd islets was then formed on the surface of Fe [71,72]. Therefore, a theoretical Pd surface coverage could be estimated by assuming a uniform distribution of the Pd monolayer on the surface of Fe [73]. Based on XRD studies, the Pd layer was found to be predominantly in the lowest energy face-centered cubic (fcc) (111) crystallographic orientation (Fig. 5a). Since each fcc (111) plane contains two Pd atoms, the surface area of single atom in the fcc (111) unit cell is calculated as:

$$\begin{aligned} Surface\ Area\ of\ Single\ Atom\ in\ Unit\ Cell,\ nm^2 &= \frac{0.5 \times 2\sqrt{3}\,r \times 4r}{2} \\ &= 2\sqrt{3}\,r^2 \end{aligned} \quad (5)$$

Where, r is the radius of a palladium atom (0.138 nm). According to the observed diameter of Fe particles in TEM (average diameter: 4.2 nm; SI section 10), the loading of a full Pd monolayer coverage on the Fe surface was derived as 53 wt% of Fe. In experiments, the Pd contents as 0.05, 0.5, 2, 5.5, 12 and 50 wt% of Fe correspond to 0.1, 1.0, 3.8, 10.4, 22.6, 94.3% Pd coverage on Fe surface, respectively. At a low surface coverage (< 10.4%, corresponding < 5.5 wt%), an increase of dechlorination and a decrease of H_2 production were observed with increasing Pd coverage. This observation indicates, when sufficient H_2 is produced at low Pd coverage (coverage from 0% to 10.4%, corresponding to 0 wt% to 5.5 wt%), the amount of catalyst Pd was the rate-limiting factor for the dechlorination reaction. However, H_2 production was observed to be the rate-limiting factor at higher Pd surface coverage (10.4–94.3%, corresponding to 5.5 wt% to 50 wt%). No significant production of H_2 was found for the 50 wt% batches, which correspond to a nearly 95% Pd coverage on the individual Fe particles. Overall, the batches with Pd percentages from 0.5 wt% to 5.5 wt% (1.0%–10.4% Pd coverage) yielded higher dechlorination performance.

The composition of the nanoparticles, either palladized-Fe bimetallic or isolated Pd and Fe particles, is another important factor for dechlorination. As shown in Fig. 6a, with 0.5 wt% Pd and a same Fe source, the palladized-Fe batches presented a significantly higher reaction rate (observed rate constant k_{obs} = 0.173 min^{-1}) than the isolated Pd and Fe batches (k_{obs} = 0.009 min^{-1}, Pd particle size ~4.5 nm (Fig. S.7a). Even when 24-fold more Pd was added as isolated particles (12 wt% Pd), the reactivity (k_{obs} = 0.014 min^{-1}) was nearly 12-fold lower than the palladized-Fe batches with only 0.5 wt% Pd. The isolated batches were observed to have insignificant effect on H_2 production (Fig. 6b), but the formation of Pd islet on the Fe surface, on the palladized-Fe batches (Fig. S.7b), enhances the specific surface area of the Pd catalyst compared to the Pd particles formed on the isolated Pd and Fe batches. The larger specific surface area contributes to a higher reaction rate for the palladized-Fe particles. Furthermore, the palladized-Fe is more favorable for the diffusion of produced H_2 to the reactive sites on Pd islets, which could increase the formation of atomic hydrogen for dechlorination.

3.2.2. Effects of pH and temperature in PCB 1 dechlorination—Environmental pH can impact the longevity of bimetallic particles and dechlorination performance [74,75]. In acidic condition, the H_2 produced via corrosion of Fe occurs more readily and thus provides more H_2 for Pd activation. In alkaline conditions, a surface passivation occurs via iron hydroxide precipitation, resulting in the formation of passive surface layer that can deactivate Pd/Fe particles [76].

The solution pH was proven to have a significant impact on PCB 1 dechlorination (Fig. 7a). The initial pH of PCB 1 solutions was adjusted to be 3.5, 7.8 and 9.2, respectively, by adding H_2SO_4 or NaOH. No buffer solutions were added to prevent any effects of buffers on corrosion of Fe [77]. After the dechlorination reaction, the water corrosion of Fe caused slight changes on pH [75], which resulted in pH values of 3.6, 8.1 and 9.3, respectively. In Fig. 7a, the higher initial dechlorination rate was observed at pH 3.5 batches. A discoloration (from black to pale green) was observed for the pH 3.5 samples after 1.5 min, which indicated the dissolution of Fe particles. Even though lower pH batches showed the faster initial dechlorination rate, they eventually produced less biphenyl than the batches at pH 7.8 and 9.2. A positive correlation between acidic condition and overall dechlorination performance was reported for similar Pd/Fe bimetallic systems [77,78]. However, the size and concentration of the bimetallic nanoparticles are important to consider and could potentially reduce dechlorination performance. The negative correlation with acidic condition and dechlorination could be explained as following: (1) extensive and rapid H_2 production could form gas bubbles around the reaction sites which inhibits dissolved-phase contact with target pollutants [75,79]; (2) Fe could be rapidly consumed when the produced H_2 is not able to efficiently activated as reactive atomic hydrogen [80]; and (3) the loss of Pd islets on Fe surface caused by the rapid erosion of Fe base [74,79].

To better understand the mechanism of the PCB 1 dechlorination reaction, kinetic studies were investigated to evaluate the activation energy (Ea, kj/mol). As shown in Fig. 7b, a higher temperature had a positive effect on the dechlorination (mass balance was achieved above 90% for every batches). The k_{obs} under temperatures of 4, 15, 23 and 40 °C were calculated as 0.076, 0.147, 0.173 and 0.291 min^{-1}, respectively. With 0.5 wt% Pd, the activation energy was found to be 26.5 kj/mol (Details in SI section 11). According to calculated activation energy, the consistency of dechlorination results between the experimental and predicted data was found and shown in Fig. S.9. Fang and Al-Abed reported the activation energy for PCB 1 dechlorination between 17 and 20 kj/mol from 4 °C to 60 °C using Pd/Fe nanoparticles (Pd was 0.585 wt% of Fe). They found an insignificant relation between the observed dechlorination rates and the initial concentration of PCB 1, which suggests the overall rate is limited by the adsorption [81]. Xu et al. reported Ea = 24.5 kj/mol for the dechlorination of 2,2′-dichlorobiphenyl by membrane-supported Pd/Fe nanoparticles suggesting a diffusion-controlled reaction [82]. An Ea of 29 kj/mol was reported for PCB 77 dechlorination at 25 and 40 °C in a Pd/Fe nanotubes system, which indicates the shape of the catalyst has some pivotal role in reaction mechanism [83]. The effect of the shape of particles on activation energy was reported considering tetrahedral, cubic and near spherical particles in solution phase [84]. The development of the FIB cross-sectioning method in section 3.1.2 could open the window to explore the roles of shapes and

other morphologies of particles on reactivity, specifically for those particles inside the polymer matrix.

3.3. Remediation of contaminated groundwater from a site

The dechlorination studies in section 3.2, using a well-studied PCB 1, evaluated the intrinsic properties of Pd/Fe nanoparticles on the reactivity. Combined with the material characterization on membrane morphology and nanoparticles on the membrane pores, the research is extended to the remediation of contaminated groundwater using the Pd/Fe nanoparticles incorporated membranes. The groundwater was collected from a contaminated industrial site, that is currently being remediated. Compared to the conventional on site-based treatment which uses sorption methods, such as air stripping, the use of catalytic membranes requires less energy consumption and could degrade the contaminants.

The groundwater contains saturated and unsaturated chlorinated aliphatic compounds, that are chloroform (CF), carbon tetrachloride (CTC), trichloroethylene (TCE) and tetrachloroethylene (PCE) (in Table 2). No significant variation in concentration of contaminants was observed between the groundwater samples collected during spring and summer in 2018. In this study, the real groundwater samples (collected on summer) were used in the treatment study in both solution phase without membranes and in membrane domain under convective flow mode (SI section 12).

3.3.1. The groundwater treatment with Pd/Fe nanoparticles—After a 30 min reaction in the solution phase studies (CMC is 0.5 wt %, [Fe] = 72 ppm and 0.5 wt% Pd), all the species were effectively dechlorinated below the threshold of EPA maximum contaminant level (Fig. 8). The control group was made using deliberately oxidized Pd/Fe nanoparticles, which were prepared by purging air into the suspension of the Pd/Fe nanoparticles for 12 h. The control group shows more than 88% remaining of every species. Less than 1% remaining was achieved for all the species except CF. The CF is the dechlorination intermediates of CTC, which leads to the increase of CF concentration in first 5 min reaction.

For chlorinated ethylenes, the complete dechlorination of TCE and PCE to nontoxic ethylene and ethane, using Pd/Fe particles, has been reported in the literature [23,24,85,86]:

$$TCE \xrightarrow{multiple\ dechlorination} ethylene\ /\ ethane + 3Cl^{-} \quad (6)$$

For chlorinated methanes, Feng and Lim reported that above 85% CTC was dechlorinated to methane, with an existence of 11% dichloromethane as a dechlorination intermediate [87]:

$$CCl_4 \xrightarrow{Pd/Fe} CH_4 + 4Cl^{-} \quad (7)$$

$$CCl_4 \xrightarrow{Pd/Fe} CH_2Cl_2 + 2Cl^{-} \quad (8)$$

To better understand the dechlorination performance, some synthetic solutions with higher initial concentration of CTC (15 ppm) and TCE (11.7 ppm) were made, for use in the chloride ion (Cl^-) measurement. The Cl^- is one of the final products of the dechlorination: the complete dechlorination of 1 mol CTC and 1 mol TCE would theoretically produce 4 mol and 3 mol Cl^-, respectively. The result shows above 99% CTC was degraded and 76% CTC was dechlorinated in 4 h (Fig. S.12). Compared to the complete dechlorination of TCE (nearly 97% conversion of chloride), the less dechlorination in CTC study indicates the incomplete dechlorination of CTC. The GC-MS results show that 8% CTC was converted to dichloromethane, whose concentration was then kept stable in this study. The incomplete dechlorination of CTC to methane has also been found [87].

Based on the degradation results, the degradation could be regarded as pseudo-first-order reaction (equation (9)). The concentration of CF initially increases due to CTC dechlorination (CF is a dechlorination intermediate of CTC). Since the degradation rate of CTC is much greater than that of CF, for ease of derivation, the degradation of CF could be regarded as pseudo-first-order reaction after the complete degradation of CTC.

$$\frac{dC}{dt} = -k_{sa}\rho_m a_s C \tag{9}$$

Where, k_{sa} is surface normalized reaction rate ($Lm^{-2}\ min^{-1}$). ρ_m is nanoparticle loading density, which is 0.072 gL^{-1}, a_s is surface area per unit mass, which is 187 m^2g^{-1}, calculated from average spherical nanoparticle size (4.2 nm, based on the TEM characterization) and iron density (7870 gL^{-1}). The summary of k_{sa} is listed in Table 3. The reduction rate followed the order of CTC > TCE > PCE > CF.

3.3.2. The groundwater treatment in the membrane domain—For the convective flow study, the groundwater was permeated through a Pd/Fe-PMAA-PVDF membrane (4.1 mg Fe, Pd was 0.5 wt% of Fe) under 0.34, 0.69 and 1.0 bar, corresponding to the 2.2 s, 1.8 s and 0.9 s residence time, respectively. Residence time is the period the species spent inside the membrane pores, which was controlled by the operating pressure and was used to determine the reaction time for dechlorination. Assuming a uniform distribution of cylindrical pores of the membranes, the residence time (τ) was derived as equations (10) and (11).

$$\tau = V_{void} / (J_w A) \tag{10}$$

$$V_{void} = V_{matrix} - V_{NP} = V_{membrane}\varnothing - V_{NP} \tag{11}$$

where J_w is the groundwater flux at specific pressure. A is membrane effective surface area. V_{matrix} is the volume inside PMAA functionalized membrane pores. $\varnothing$ is the surface porosity and it was measured using SEM (SI section 7). V_{NP} is the volume of Pd/Fe particles, which was calculated using the specific metal loading (measured using ICP). The details of derivation were explained in SI section 13.

The permeate samples at different operating pressures were collected after 15 min to allow the system to reach a steady state. The control group, using the oxidized Pd/Fe-PMAA-PVDF membranes, was made to test the potential loss due to adsorption and evaporation. The membranes were deliberately oxidized by immersing into the water with purging air for 12 h. As shown in Fig. 9a, the concentration of chlorinated species declined continuously with the increase of residence times. The initial pH 7.8 was increased to 8.0, 8.0 and 8.2 at the residence times of 0.9 s, 1.8 s and 2.2 s, respectively. At 2.2 s residence time in a single pass through the membranes, only 25% CF, 1% CTC, 9% TCE and 16% PCE remained. The extent of dechlorination could be modulated by varying the operating pressure gradient across the membrane.

In addition, the functionalization of PMAA prevents leaching of embedded nanoparticles. Although the dechlorination reaction and the corrosion in water convert Fe^0 to Fe^{2+}, the PMAA chains serve as a cation exchanger and recapture the leached Fe^{2+}. To test the stability of Pd/Fe nanoparticles on the membrane domains, the 200 ml contaminated groundwater samples were pressurized through the membranes at 1 bar (equivalent of 179 L/m^2 flow through membrane). Results show less than 2% Fe and Pd, compared to the metal loading on the membranes, were leached and found in the permeate solution using ICP.

Based on the characterization of membrane pores (pore size: 60.6 ± 16.7 nm), the assumption of uniform and cylindrical pores was made. A plug flow reactor model was then used to obtain the rate constant. For instance, the rate of TCE dechlorination k_{obs}, at residence time of 0.9 s, 1.8 s and 2.2 s, was determined to be 0.93 s^{-1}, 0.80 s^{-1} and 0.89 s^{-1}, respectively. The average k_{obs} was calculated as 0.87 s^{-1}. With the characterization of membrane porosity and nanoparticles inside the membrane pores (particle size of 17.1 ± 4.9 nm, in Fig. S.6e), the k_{sa} value of TCE in convective flow mode, with 0.5 wt% Pd, was calculated as 0.009 $Lm^{-2}min^{-1}$. Compared to the solution phase studies, the same trend of degradation rate was observed as: CTC > TCE > PCE > CF (in Table 3). Moreover, the significant decline of k_{sa} from the solution phase studies to the membrane domain studies (besides CF) indicates the diffusion-controlled reaction in the membrane domain. Compared to the well mixed solution phase, the membrane domain causes additional mass transfer resistance, which hinders the diffusion of contaminants to reactive nanoparticles and decreases the observed reaction rate. For CF, the k_{sa} is much lower than the other compounds and the difference between the two studies could within the margin of experimental error.

As shown in Fig. 9b, an increase of $[Cl^-]$ in the permeate samples was found using a chloride electrode (details in SI section 12). Based on the GC-MS results, the theoretical $[Cl^-]$ production should be 1.2 ppm (34 μM) when all the four chlorinated compounds were completely dechlorinated. The chloride production was found to be 4–5 folds greater than the theoretical amount. Besides the target compounds, other volatile chlorinated compounds were also found in the groundwater included ~196 ppb 1,2-dichloroethene, ~82 ppb hexachlorobutadiene and ~200 ppb hexachloroethane. These three volatile compounds were also demonstrated to dechlorinate with Pd/Fe and accounts for some of the difference in chloride mass balance [88,89]. Since the analysis in this study was focused only on the target volatile chlorinated contaminants, the column used in GC was specific for the

detection of volatile compounds. The possible presence of other larger chlorinated organic molecules and non-volatile species was not validated (no chlorobenzene was found using semi-volatile column). Thus, the measurement of produced [Cl^-] could reflect the overall trend of dechlorination but could not be used as an appropriate indicator for the dechlorination extent of individual chlorinated organics. However, due to the low cost and the benefit from real-time sensing capability, the chloride electrode could be used as a monitor for the dechlorination performance on site.

3.3.3. Long-term convective flow study in the membrane domain—To test the commercial viability of the functionalized membranes, a long-term study was conducted using the synthetic water of model compounds, such as CTC and PCE (35 ppb CTC and 950 ppb PCE as the similar concentrations as the target groundwater, pH was also adjusted to 7.8). The Pd/Fe-PMAA-PVDF membranes (12.1 wt% PMAA, permeability: 25 LMH/bar) was tested in a continuous flow with the operating pressure of 0.34 bar, which indicates a residence time of 2.2 s. The deliberately oxidized Pd/Fe-PMAA-PVDF membranes were used as control group. As shown in Fig. 10a, a consistent degradation performance was observed within first 5 h, that is less than 5% CTC and 20% PCE were remained in the permeate samples. A significant decrease of reactivity was observed after 36 h continuous flow (equivalent of treatment of 299 L/m^2). Compared to the reactive nanoparticles for initial condition (Fig. 10b), several sheet-like structures (15–105 nm in length) were observed after 36 h continuous flow (Fig. 10c), which might indicate the formation of iron oxide or iron hydroxide. This formation of passive layer could hinder the degradation reactions [69,90]. However, the regeneration of nanoparticles was achieved by passing $NaBH_4$ (210 mol% of initial [Fe]) through the membranes. After regeneration and washing using deoxygenated DI water, a recovery of reactivity was observed and a similar degradation performance was achieved compared to the first cycle. The control group was also regenerated but then oxidized again by passing DI water using air for the operating pressure. Particle size on the membrane surface was changed from 20.1 ± 7.2 nm (at t = 0 h) to 26.2 ± 5.2 nm after regeneration (Fig. 10d). No severe agglomeration of nanoparticles was observed. Furthermore, the capacity of PMAA to recapture the dissolved iron ions (discussed on section 3.3.2) could retain the iron ions for further conversion to Fe^0.

4. Conclusion

The Pd/Fe-PMAA-PVDF membranes were synthesized using less volatile monomer – methacrylic acid. The formation of PMAA in membrane pores prevents agglomeration (particle size of 26.2 ± 5.2 nm after a 36 h continuous flow and following $NaBH_4$ reduction) and leaching of the incorporated nanoparticles (< 2% leached after passing 179 L/m^2 equivalent of water through the membranes at 1 bar). A uniform distribution of particle size (17.1 ± 4.9 nm) and density at entire PVDF layer of the membrane were observed using the developed FIB cross-sectioning method.

The intrinsic properties of Pd/Fe particles were evaluated by the measurement of H_2 production and corresponding dechlorination performance. Pd with face-centered cubic structure was observed on the Fe surface using TEM and XRD. Since hydrogen production is from iron corrosion one would expect lower production as Pd coverage is increased, and

this was indeed observed. The H_2 production was observed to become the rate limiting factor on dechlorination performance at higher coverage (10.4–94.3%, corresponding to 5.5 to 50 wt% Pd of Fe). Palladized-Fe presented faster dechlorination rate: k_{obs} is 18-fold higher than isolated Pd and Fe nanoparticles (Pd is 0.5 wt% of Fe in both cases). In addition, the activation energy of PCB 1 dechlorination is 26.5 kJ/mol, at pH 7.8, using 0.5 wt% Pd.

The groundwater samples were dechlorinated using the Pd/Fe-PMAA-PVDF membranes. A single pass through the membrane (0.5 wt % Pd, 99.5% Fe) lowered feed concentrations by 75% CF, 99% CTC, 91% TCE and 84% PCE at a residence time of only 2.2 seconds. The reduction rate followed the order of CTC > TCE > PCE > CF. The decline of k_{sa} from the solution phase studies to the membrane domain studies indicates the role of polymer-pollutant partitioning and channeling effects. A synthetic water was also prepared for a long-term study. The study shows less than 5% CTC and 20% PCE were remained in a continuous flow through the membranes within first 5 h. The regeneration using $NaBH_4$ recovered the reactivity after a significant decrease of degradation performance after 36 h continuous flow (equivalent of 299 L/m^2 treatment of water).

Supplementary Material

Refer to Web version on PubMed Central for supplementary material.

Acknowledgement

This work is supported by the NIEHS-SRP grant P42ES007380. Partial support is also provided by NSF KY EPSCoR grant (Grant no: 1355438). We appreciate the suggestions and the work of Dr. Sebastian Hernandez. We thank John May and Megan Combs from Environmental Research and Training Laboratory (ERTL) at UK for analytical assistance. We also appreciate the help provided by Paul Lee (Undergraduate Chemical Engineering Student) with some of the experiments on chlorinated organics.

References

[1]. Park HB, Kamcev J, Robeson LM, Elimelech M, Freeman BD, Maximizing the right stuff: the trade-off between membrane permeability and selectivity, Science 356 (2017) eaab0530. [PubMed: 28619885]

[2]. Logan BE, Elimelech M, Membrane-based processes for sustainable power generation using water, Nature 488 (2012) 313. [PubMed: 22895336]

[3]. Bae TH, Lee JS, Qiu W, Koros WJ, Jones CW, Nair S, A high-performance gas-separation membrane containing submicrometer-sized metal–organic framework crystals, Angew. Chem. Int. Ed 49 (2010) 9863–9866.

[4]. Shen Y.-x., Saboe PO, Sines IT, Erbakan M, Kumar M, Biomimetic membranes: a review, J. Membr. Sci 454 (2014) 359–381.

[5]. Karan S, Jiang Z, Livingston AG, Sub–10 nm polyamide nanofilms with ultrafast solvent transport for molecular separation, Science 348 (2015) 1347–1351. [PubMed: 26089512]

[6]. Zeman LJ, Zydney AL, Microfiltration and Ultrafiltration: Principles and Applications, CRC Press, 2017.

[7]. Wei J, Qiu C, Tang CY, Wang R, Fane AG, Synthesis and characterization of flat-sheet thin film composite forward osmosis membranes, J. Membr. Sci 372 (2011) 292–302.

[8]. Hu C, Wang M-S, Chen C-H, Chen Y-R, Huang P-H, Tung K-L, Phosphorus-doped g-C3N4 integrated photocatalytic membrane reactor for wastewater treatment, J. Membr. Sci 580 (2019) 1–11.

[9]. Fang X, Li J, Ren B, Huang Y, Wang D, Liao Z, Li Q, Wang L, Dionysiou DD, Polymeric ultrafiltration membrane with in situ formed nano-silver within the inner pores for simultaneous separation and catalysis, J. Membr. Sci 579 (2019) 190–198.

[10]. Ling R, Shao J, Chen JP, Reinhard M, Iron catalyzed degradation of an aromatic polyamide reverse osmosis membrane by free chlorine, J. Membr. Sci 577 (2019) 205–211.

[11]. Vitola G, Mazzei R, Poerio T, Porzio E, Manco G, Perrotta I, Militano F, Giorno L, Biocatalytic membrane reactor development for organophosphates degradation, J. Hazard Mater 365 (2019) 789–795. [PubMed: 30476802]

[12]. Zhang H, Luo J, Li S, Woodley JM, Wan Y, Can graphene oxide improve the performance of biocatalytic membrane? Chem. Eng. J 359 (2019) 982–993.

[13]. Wang X, Zou Y, Meng B, Tan X, Wang S, Liu S, Catalytic palladium membrane reactors for one-step benzene hydroxylation to phenol, J. Membr. Sci 563 (2018) 864–872.

[14]. Sun M, Zucker I, Davenport DM, Zhou X, Qu J, Elimelech M, Reactive, self-cleaning ultrafiltration membrane functionalized with iron oxychloride nanocatalysts, Environ. Sci. Technol 52 (2018) 8674–8683. [PubMed: 30004682]

[15]. Molinari R, Lavorato C, Argurio P, Recent progress of photocatalytic membrane reactors in water treatment and in synthesis of organic compounds. A review, Catalysis Today 281 (2017) 144–164.

[16]. Gul S, Rehan ZA, Khan SA, Akhtar K, Khan MA, Khan M, Rashid MI, Asiri AM, Khan SB, Antibacterial PES-CA-Ag2O nanocomposite supported Cu nanoparticles membrane toward ultrafiltration, BSA rejection and reduction of nitrophenol, J. Mol. Liq 230 (2017) 616–624.

[17]. Martinez J, Ortiz A, Ortiz I, State-of-the-art and perspectives of the catalytic and electrocatalytic reduction of aqueous nitrates, Appl. Catal. B Environ 207 (2017) 42–59.

[18]. Qing W, Li X, Shao S, Shi X, Wang J, Feng Y, Zhang W, Zhang W, Polymeric catalytically active membranes for reaction-separation coupling: a review, J. Membr. Sci 583 (2019) 118–138.

[19]. Celik G, Ailawar SA, Sohn H, Tang Y, Tao FF, Miller JT, Edmiston PL, Ozkan US, Swellable organically modified silica (SOMS) as a catalyst scaffold for catalytic treatment of water contaminated with trichloroethylene, ACS Catal. 8 (2018) 6796–6809.

[20]. Jha K, Liu Z, Vijwani H, Nadagouda M, Mukhopadhyay S, Tsige M, Carbon nanotube based groundwater remediation: the case of trichloroethylene, Molecules 21 (2016) 953.

[21]. Wu M, Xu X, Lu K, Li X, Effects of the presence of nanoscale zero-valent iron on the degradation of polychlorinated biphenyls and total organic carbon by sediment microbial fuel cell, Sci. Total Environ 656 (2019) 39–44. [PubMed: 30502733]

[22]. Wang F, Wong CS, Chen D, Lu X, Wang F, Zeng EY, Interaction of toxic chemicals with microplastics: a critical review, Water Res. 139 (2018) 208–219. [PubMed: 29653356]

[23]. Wang X, Wang W, Lowry G, Li X, Guo Y, Li T, Preparation of palladized carbon nanotubes encapsulated iron composites: highly efficient dechlorination for trichloroethylene and low corrosion of nanoiron, R. Soc. Open Sci 5 (2018) 172242. [PubMed: 30110440]

[24]. Han Y, Liu C, Horita J, Yan W, Trichloroethene hydrodechlorination by Pd-Fe bimetallic nanoparticles: solute-induced catalyst deactivation analyzed by carbon isotope fractionation, Appl. Catal. B Environ 188 (2016) 77–86.

[25]. Shi Q, Wang H, Liu S, Pang L, Bian Z, Electrocatalytic reduction-oxidation of chlorinated phenols using a nanostructured Pd-Fe modified graphene catalyst, Electrochim. Acta 178 (2015) 92–100.

[26]. Jovanovic GN, Atwater JE, Žnidaršič-Plazl P, Plazl I, Dechlorination of polychlorinated phenols on bimetallic Pd/Fe catalyst in a magnetically stabilized fluidized bed, Chem. Eng. J 274 (2015) 50–60.

[27]. Ma Y, Wang Y, Lv X, Meng F, Yang Q, Insight into the mode of action of Pd-doped zero-valent iron nanoparticles@ graphene (Pd/FePs@ G) toward carbon tetrachloride dechlorination reaction in aqueous solution, Appl. Catal. Gen 560 (2018) 84–93.

[28]. Elliott DW, Zhang W-X, Field assessment of nanoscale bimetallic particles for groundwater treatment, Environ. Sci. Technol 35 (2001) 4922–4926. [PubMed: 11775172]

[29]. He F, Zhao D, Paul C, Field assessment of carboxymethyl cellulose stabilized iron nanoparticles for in situ destruction of chlorinated solvents in source zones, Water Res. 44 (2010) 2360–2370. [PubMed: 20106501]

[30]. Su C, Puls RW, Krug TA, Watling MT, O'Hara SK, Quinn JW, Ruiz NE, A two and half-year-performance evaluation of a field test on treatment of source zone tetrachloroethene and its chlorinated daughter products using emulsified zero valent iron nanoparticles, Water Res. 46 (2012) 5071–5084. [PubMed: 22868086]

[31]. O'Carroll D, Sleep B, Krol M, Boparai H, Kocur C, Nanoscale zero valent iron and bimetallic particles for contaminated site remediation, Adv. Water Resour 51 (2013) 104–122.

[32]. Grieger KD, Fjordøge A, Hartmann NB, Eriksson E, Bjerg PL, Baun A, Environmental benefits and risks of zero-valent iron nanoparticles (nZVI) for in situ remediation: risk mitigation or trade-off? J. Contam. Hydrol 118 (2010) 165–183. [PubMed: 20813426]

[33]. Zhao X, Liu W, Cai Z, Han B, Qian T, Zhao D, An overview of preparation and applications of stabilized zero-valent iron nanoparticles for soil and groundwater remediation, Water Res. 100 (2016) 245–266. [PubMed: 27206054]

[34]. Wilson S, Greenlee LF, Post-synthesis separation and storage of zero-valent iron nanoparticles, J. Nanosci. Nanotechnol 17 (2017) 2413–2422. [PubMed: 29648431]

[35]. Torrey JD, Killgore JP, Bedford NM, Greenlee LF, Oxidation behavior of zero-valent iron nanoparticles in mixed matrix water purification membranes, Environ. Sci.: Water Res. Technol 1 (2015) 146–152.

[36]. Zhang D, Li Y, Tong S, Jiang X, Wang L, Sun X, Li J, Liu X, Shen J, Biochar supported sulfide-modified nanoscale zero-valent iron for the reduction of nitrobenzene, RSC Adv. 8 (2018) 22161–22168.

[37]. Parshetti GK, Doong R.-a., Dechlorination of trichloroethylene by Ni/Fe nanoparticles immobilized in PEG/PVDF and PEG/nylon 66 membranes, Water Res. 43 (2009) 3086–3094. [PubMed: 19476967]

[38]. Wang X, Chen C, Liu H, Ma J, Preparation and characterization of PAA/PVDF membrane-immobilized Pd/Fe nanoparticles for dechlorination of trichloroacetic acid, Water Res. 42 (2008) 4656–4664. [PubMed: 18775551]

[39]. Li X, Sotto A, Li J, Van der Bruggen B, Progress and perspectives for synthesis of sustainable antifouling composite membranes containing in situ generated nanoparticles, J. Membr. Sci 524 (2017) 502–528.

[40]. Ng LY, Mohammad AW, Leo CP, Hilal N, Polymeric membranes incorporated with metal/metal oxide nanoparticles: a comprehensive review, Desalination 308 (2013) 15–33.

[41]. Kim J, Van der Bruggen B, The use of nanoparticles in polymeric and ceramic membrane structures: review of manufacturing procedures and performance improvement for water treatment, Environ. Pollut 158 (2010) 2335–2349. [PubMed: 20430495]

[42]. Zodrow K, Brunet L, Mahendra S, Li D, Zhang A, Li Q, Alvarez PJ, Polysulfone ultrafiltration membranes impregnated with silver nanoparticles show improved biofouling resistance and virus removal, Water Res. 43 (2009) 715–723. [PubMed: 19046755]

[43]. Cheng M.-m., Huang L.-j., Wang Y.-x., Tang J.-g., Wang Y, Zhao Y.-c., Liu G.-f., Zhang Y, Kipper MJ, Wickramasinghe SR, Reduced graphene oxide–gold nanoparticle membrane for water purification, Separ. Sci. Technol 54 (2019) 1079–1085.

[44]. Wang X, Zhu M, Liu H, Ma J, Li F, Modification of Pd–Fe nanoparticles for catalytic dechlorination of 2, 4-dichlorophenol, Sci. Total Environ 449 (2013) 157–167. [PubMed: 23425792]

[45]. Chitpong N, Husson S, Nanofiber ion-exchange membranes for the rapid uptake and recovery of heavy metals from water, Membranes 6 (2016) 59.

[46]. Chitpong N, Husson SM, Polyacid functionalized cellulose nanofiber membranes for removal of heavy metals from impaired waters, J. Membr. Sci 523 (2017) 418–429.

[47]. Smuleac V, Varma R, Sikdar S, Bhattacharyya D, Green synthesis of Fe and Fe/Pd bimetallic nanoparticles in membranes for reductive degradation of chlorinated organics, J. Membr. Sci 379 (2011) 131–137.

[48]. Xia Z, Liu H, Wang S, Meng Z, Ren N, Preparation and dechlorination of a poly (vinylidene difluoride)-grafted acrylic acid film immobilized with Pd/Fe bimetallic nanoparticles for monochloroacetic acid, Chem. Eng. J 200 (2012) 214–223.

[49]. Islam MS, Hernández S, Wan H, Ormsbee L, Bhattacharyya D, Role of membrane pore polymerization conditions for pH responsive behavior, catalytic metal nanoparticle synthesis, and PCB degradation, J. Membr. Sci 555 (2018) 348–361.

[50]. Yahia Cherif A, Arous O, Mameri N, Zhu J, Ammi Said A, Vankelecom I, Simoens K, Bernaerts K, Van der Bruggen B, Fabrication and characterization of novel antimicrobial thin film nano-composite membranes based on copper nanoparticles, J. Chem. Technol. Biotechnol 93 (2018) 2737–2747.

[51]. Hu Y, Lü Z, Wei C, Yu S, Liu M, Gao C, Separation and antifouling properties of hydrolyzed PAN hybrid membranes prepared via in-situ sol-gel SiO2 nanoparticles growth, J. Membr. Sci 545 (2018) 250–258.

[52]. Wan H, Briot NJ, Saad A, Ormsbee L, Bhattacharyya D, Pore functionalized PVDF membranes with in-situ synthesized metal nanoparticles: material characterization, and toxic organic degradation, J. Membr. Sci 530 (2017) 147–157.

[53]. Giannuzzi LA, Stevie FA, A review of focused ion beam milling techniques for TEM specimen preparation, Micron 30 (1999) 197–204.

[54]. Lee JZ, Wynn TA, Schroeder MA, Alvarado J, Wang X, Xu K, Meng YS, Cryogenic focused ion beam characterization of lithium metal anodes, ACS Energy Lett. 4 (2019) 489–493.

[55]. Jiang J, Fu C, Zhao D, Kinetics of 2-chlorobiphenyl reductive dechlorination by Pd-fe0 nanoparticles, MATEC Web of Conferences, EDP Sciences, 201605021.

[56]. He F, Zhao D, Hydrodechlorination of trichloroethene using stabilized Fe-Pd nanoparticles: reaction mechanism and effects of stabilizers, catalysts and reaction conditions, Appl. Catal. B Environ 84 (2008) 533–540.

[57]. Dong T, Luo H, Wang Y, Hu B, Chen H, Stabilization of Fe–Pd bimetallic nanoparticles with sodium carboxymethyl cellulose for catalytic reduction of para-nitrochlorobenzene in water, Desalination 271 (2011) 11–19.

[58]. Liu M, Huang R, Li C, Che M, Su R, Li S, Yu J, Qi W, He Z, Continuous rapid dechlorination of p-chlorophenol by Fe-Pd nanoparticles promoted by procyanidin, Chem. Eng. Sci 201 (2019) 121–131.

[59]. Qin L, Mergos IA, Verweij H, Obtaining accurate cross-section images of supported polymeric and inorganic membrane structures, J. Membr. Sci 476 (2015) 194–199.

[60]. Pérez JH, López-Ruiz B, López-Cabarcos E, Synthesis and characterization of microparticles based on poly-methacrylic acid with glucose oxidase for biosensor applications, Talanta 149 (2016) 310–318. [PubMed: 26717846]

[61]. Cheng B, Li Z, Li Q, Ju J, Kang W, Naebe M, Development of smart poly (vinylidene fluoride)-graft-poly (acrylic acid) tree-like nanofiber membrane for pH-responsive oil/water separation, J. Membr. Sci 534 (2017) 1–8.

[62]. Fan X-X, Xie R, Zhao Q, Li X-Y, Ju X-J, Wang W, Liu Z, Chu L-Y, Dual pH-responsive smart gating membranes, J. Membr. Sci 555 (2018) 20–29.

[63]. Wang Y, Wang J, Yuan Z, Han H, Li T, Li L, Guo X, Chitosan cross-linked poly (acrylic acid) hydrogels: drug release control and mechanism, Colloids Surfaces B Biointerfaces 152 (2017) 252–259. [PubMed: 28119220]

[64]. Himstedt HH, Du H, Marshall KM, Wickramasinghe SR, Qian X, pH responsive nanofiltration membranes for sugar separations, Ind. Eng. Chem. Res 52 (2013) 9259–9269.

[65]. Nutt MO, Hughes JB, Wong MS, Designing Pd-on-Au bimetallic nanoparticle catalysts for trichloroethene hydrodechlorination, Environ. Sci. Technol 39 (2005) 1346–1353. [PubMed: 15787376]

[66]. Wang S, Yang B, Zhang T, Yu G, Deng S, Huang J, Catalytic hydrodechlorination of 4-chlorophenol in an aqueous solution with Pd/Ni catalyst and formic acid, Ind. Eng. Chem. Res 49 (2010) 4561–4565.

[67]. Chaplin BP, Reinhard M, Schneider WF, Schüth C, Shapley JR, Strathmann TJ, Werth CJ, Critical review of Pd-based catalytic treatment of priority contaminants in water, Environ. Sci. Technol 46 (2012) 3655–3670. [PubMed: 22369144]

[68]. Tee Y-H, Bachas L, Bhattacharyya D, Degradation of trichloroethylene by iron-based bimetallic nanoparticles, J. Phys. Chem. C 113 (2009) 9454–9464.

[69]. Su J, Lin S, Chen Z, Megharaj M, Naidu R, Dechlorination of p-chlorophenol from aqueous solution using bentonite supported Fe/Pd nanoparticles: synthesis, characterization and kinetics, Desalination 280 (2011) 167–173.

[70]. Choi H, Al-Abed SR, Agarwal S, Dionysiou DD, Synthesis of reactive nano-Fe/Pd bimetallic system-impregnated activated carbon for the simultaneous adsorption and dechlorination of PCBs, Chem. Mater 20 (2008) 3649–3655.

[71]. Haham H, Grinblat J, Sougrati M-T, Stievano L, Margel S, Engineering of air-stable Fe/C/Pd composite nanoparticles for environmental remediation applications, J. Magn. Magn. Mater 389 (2015) 82–89.

[72]. Yan W, Herzing AA, Li X.-q., Kiely CJ, Zhang W.-x., Structural evolution of Pd-doped nanoscale zero-valent iron (nZVI) in aqueous media and implications for particle aging and reactivity, Environ. Sci. Technol 44 (2010) 4288–4294. [PubMed: 20446741]

[73]. Bransfield SJ, Cwiertny DM, Roberts AL, Fairbrother DH, Influence of copper loading and surface coverage on the reactivity of granular iron toward 1, 1, 1-trichloroethane, Environ. Sci. Technol 40 (2006) 1485–1490. [PubMed: 16568760]

[74]. Zhou T, Li Y, Lim T-T, Catalytic hydrodechlorination of chlorophenols by Pd/Fe nanoparticles: comparisons with other bimetallic systems, kinetics and mechanism, Separ. Purif. Technol 76 (2010) 206–214.

[75]. Wang X, Chen C, Chang Y, Liu H, Dechlorination of chlorinated methanes by Pd/Fe bimetallic nanoparticles, J. Hazard Mater 161 (2009) 815–823. [PubMed: 18513856]

[76]. Huang G, Wang M, Hu Y, Cheng J, Lv S, Yang K, Reductive degradation of 2, 2′, 4, 4′-tretrabromodiphenyl ether with PAC-Pd/Fe nanoparticles: effects of Pd loading, initial pH and HA, and degradation pathway, Chem. Eng. J 334 (2018) 1252–1259.

[77]. Fang Y, Al-Abed SR, Correlation of 2-chlorobiphenyl dechlorination by Fe/Pd with iron corrosion at different pH, Environ. Sci. Technol 42 (2008) 6942–6948. [PubMed: 18853813]

[78]. Chen J-L, Al-Abed SR, Ryan JA, Li Z, Effects of pH on dechlorination of trichloroethylene by zero-valent iron, J. Hazard Mater 83 (2001) 243–254. [PubMed: 11348735]

[79]. Jovanovic GN, Žnidaršič-Plazl P, Sakrittichai P, Al-Khaldi K, Dechlorination of p-chlorophenol in a microreactor with bimetallic Pd/Fe catalyst, Ind. Eng. Chem. Res 44 (2005) 5099–5106.

[80]. Jia H, Gu C, Li H, Fan X, Li S, Wang C, Effect of groundwater geochemistry on pentachlorophenol remediation by smectite-templated nanosized Pd 0/Fe 0, Environ. Sci. Pollut. Control Ser 19 (2012) 3498–3505.

[81]. Fang Y, Al-Abed SR, Dechlorination kinetics of monochlorobiphenyls by Fe/Pd: effects of solvent, temperature, and PCB concentration, Appl. Catal. B Environ 78 (2008) 371–380.

[82]. Xu J, Bhattacharyya D, Fe/Pd nanoparticle immobilization in microfiltration membrane pores: synthesis, characterization, and application in the dechlorination of polychlorinated biphenyls, Ind. Eng. Chem. Res 46 (2007) 2348–2359.

[83]. Zahran EM, Bhattacharyya D, Bachas LG, Reactivity of Pd/Fe bimetallic nanotubes in dechlorination of coplanar polychlorinated biphenyls, Chemosphere 91 (2013) 165–171. [PubMed: 23332879]

[84]. Narayanan R, El-Sayed MA, Shape-dependent catalytic activity of platinum nanoparticles in colloidal solution, Nano Lett. 4 (2004) 1343–1348.

[85]. Zhang W.-x., Wang C-B, Lien H-L, Treatment of chlorinated organic contaminants with nanoscale bimetallic particles, Catal. Today 40 (1998) 387–395.

[86]. Hernández S, Lei S, Rong W, Ormsbee L, Bhattacharyya D, Functionalization of flat sheet and hollow fiber microfiltration membranes for water applications, ACS Sustain. Chem. Eng 4 (2015) 907–918. [PubMed: 29392097]

[87]. Feng J, Lim T-T, Iron-mediated reduction rates and pathways of halogenated methanes with nanoscale Pd/Fe: analysis of linear free energy relationship, Chemosphere 66 (2007) 1765–1774. [PubMed: 16899274]

[88]. Wu D, Liu Y, Liu Z, Ma L, Dechlorination of hexachloroethane in water using iron shavings and amended iron shavings: kinetics and pathways, J. Chem (2014) 1–9 2014.

[89]. Rodrigues R, Betelu S.p., Colombano S.f., Masselot G, Tzedakis T, Ignatiadis I, Reductive dechlorination of hexachlorobutadiene by a Pd/Fe microparticle suspension in dissolved lactic acid polymers: degradation mechanism and kinetics, Ind. Eng. Chem. Res 56 (2017) 12092–12100.

[90]. Sayed FN, Polshettiwar V, Facile and sustainable synthesis of shaped iron oxide nanoparticles: effect of iron precursor salts on the shapes of iron oxides, Sci. Rep 5 (2015) 9733. [PubMed: 25939969]

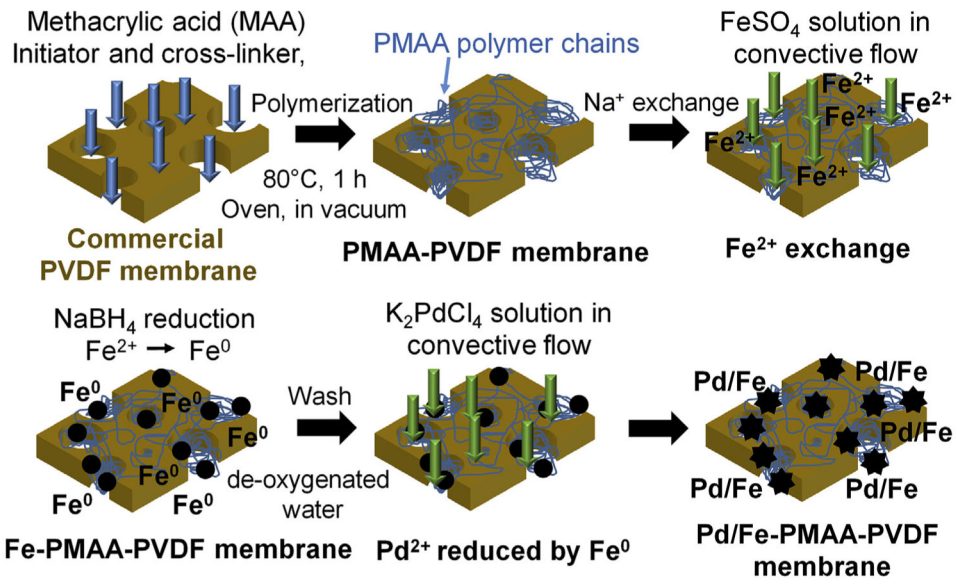

Fig. 1.

Schematic of the synthesis procedures of Pd/Fe-PMAA-PVDF membranes.

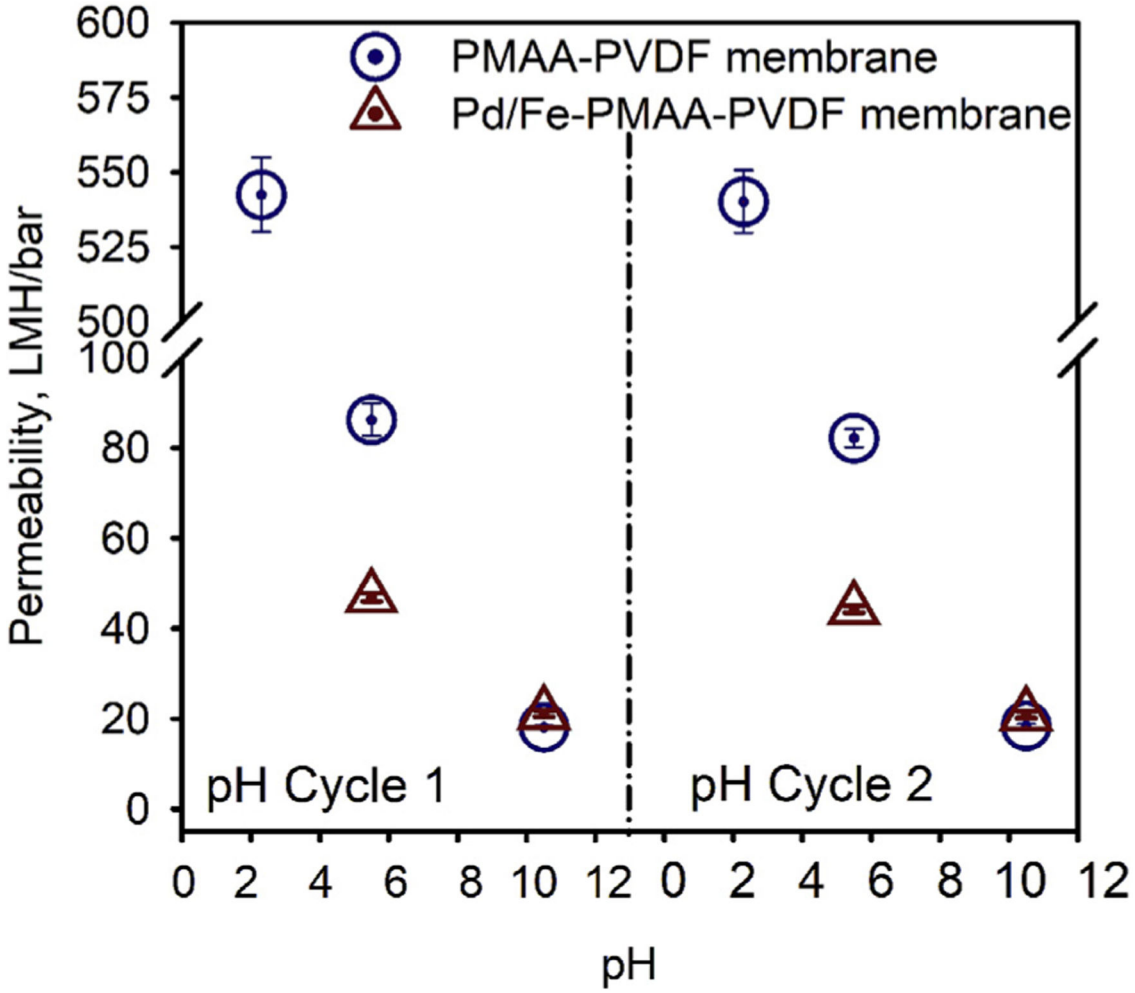

Fig. 2.

The pH-responsive permeability of two types of functionalized PVDF membranes (Solecta PVDF 700): (1) 12.1 wt% PMAA-PVDF membranes and (2) Pd/Fe particles incorporated PMAA-PVDF membranes (4.1 mg Fe, 0.5 wt% Pd). Due to the dissolution of Fe particles, the permeability at pH 2.3 was not tested. All the membranes were permeated through with target pH solution for 2 h (DI water adjusted with H_2SO_4 or NaOH) to reach steady state.

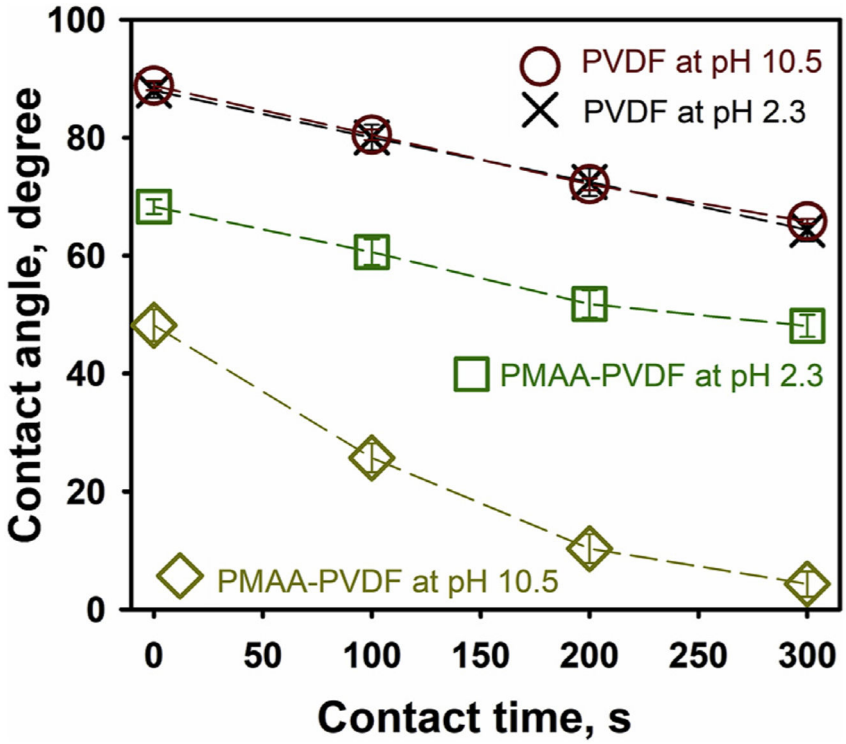

Fig. 3.

The change of contact angles as a function of contact time. The original PVDF membranes (Solecta PVDF 700) were used as a control for the functionalized PMAA-PVDF membranes (12.1 wt% PMAA). The membranes were immersed at target pH and then dried under a nitrogen flow before the contact angle measurement.

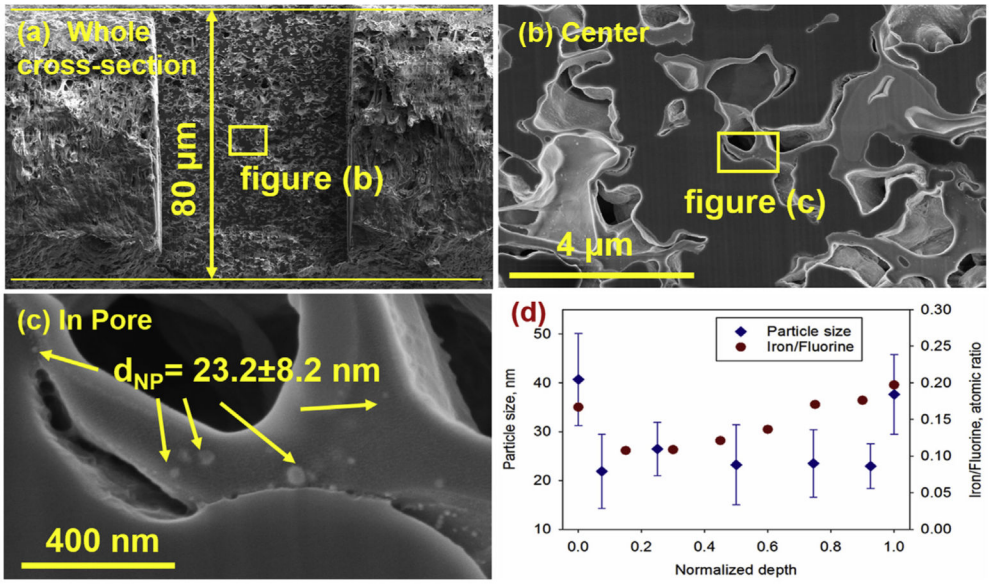

Fig. 4.

The SEM images for nanoparticles in the pores of membranes (PMAA functionalized Millipore DVPP04700 membranes). (a) An 80 μm membrane cross-section sample, the smooth area in the center, was prepared using FIB. (b) pore structure. (c) The nanoparticles inside the pores. (d) The quantification of particle size and distribution at various depths underneath the membrane surface (more than 300 particles were counted in every point). The Millipore PVDF membranes were used only for characterization.

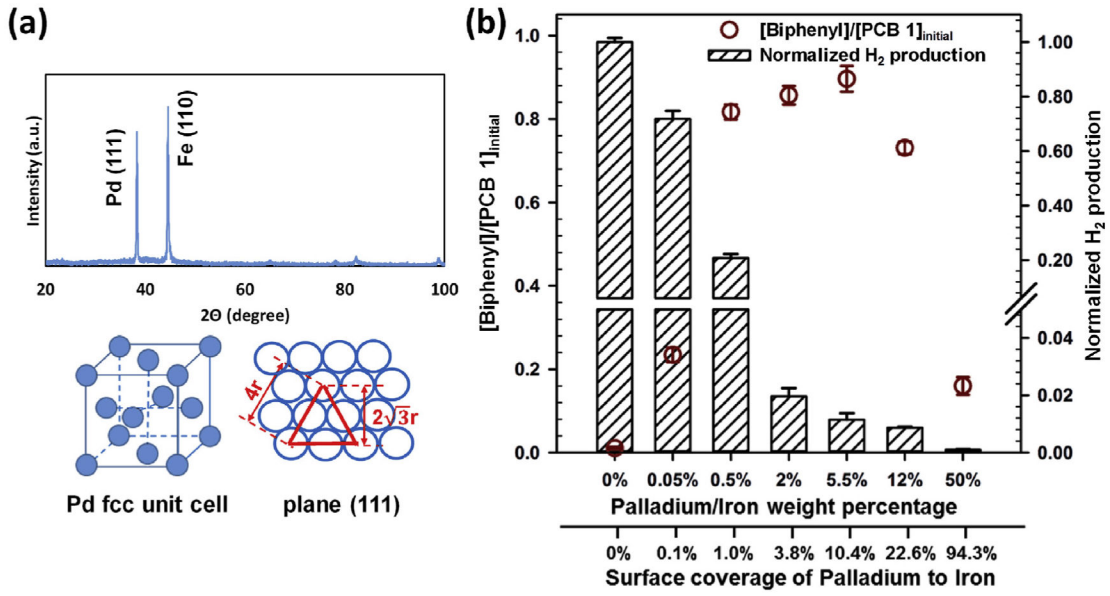

Fig. 5.

(a) XRD analysis of Pd/Fe bimetallic particles (> 100 nm particles were synthesized specifically for XRD analysis). **(b)** Solution phase studies of the effects of Pd contents (validated using ICP) on both the dechlorination and the H_2 production (CMC is 0.5 wt%, [Fe] = 500 ppm, $[PCB\ 1]_o$ = 5 ppm. Reaction time 10 min. T = 23 °C, pH = 7.8). The H_2 production at various Pd contents was normalized with the H_2 production at 0% Pd batches, which was measured as 51.2×10^{-7} mol. The mass balance between unreacted PCB 1 and produced biphenyl was achieved above 90% for every batch.

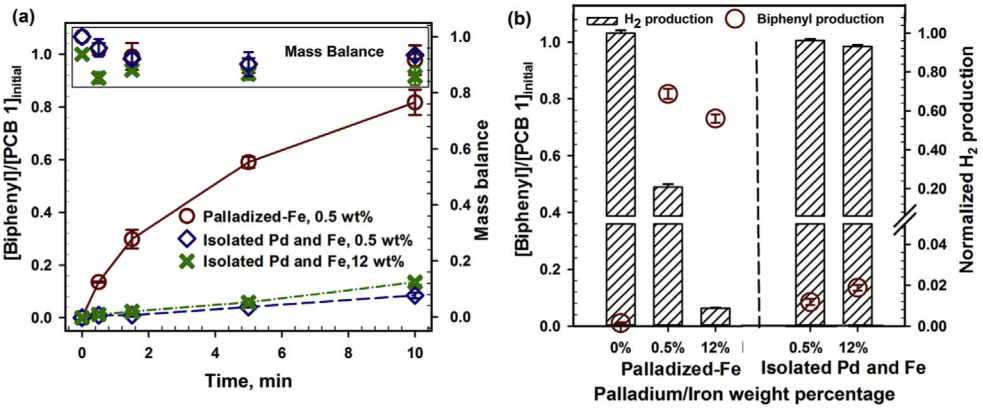

Fig. 6.

The effects of the particle composition (either palladized-Fe bimetallic or isolated Pd and Fe nanoparticles) on dechlorination (figure a) and H_2 production (figure b). This study conducted in a solution phase (CMC is 0.5 wt%, [Fe] = 500 ppm, $[PCB\ 1]_o$ = 5 ppm. T = 23 °C, pH = 7.8). The H_2 production at different Pd contents, in 10 min, was normalized with the production at 0% Pd batches.

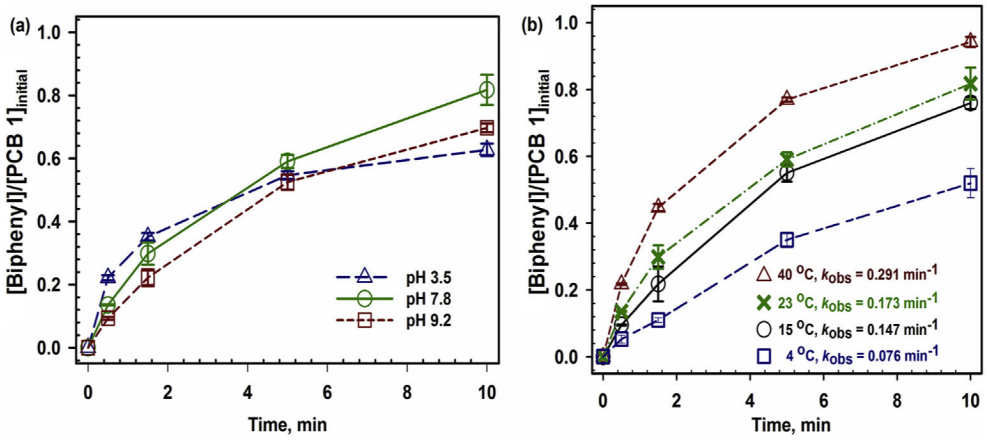

Fig. 7.

Effects of pH and temperature conditions on dechlorination performance in solution phase studies (CMC is 0.5 wt%, [Fe] = 500 ppm, Pd was 0.5 wt% of Fe, $[PCB\ 1]_o$ = 5 ppm). (a) The initial pH 3.5, 7.8 and 9.2 were converted to 3.6, 8.1 and 9.3, respectively. T = 23 °C. (b) Based on the Arrhenius equation, the activation energy of PCB 1 dechlorination was obtained as 26.5 kJ/mol. The initial pH = 7.8.

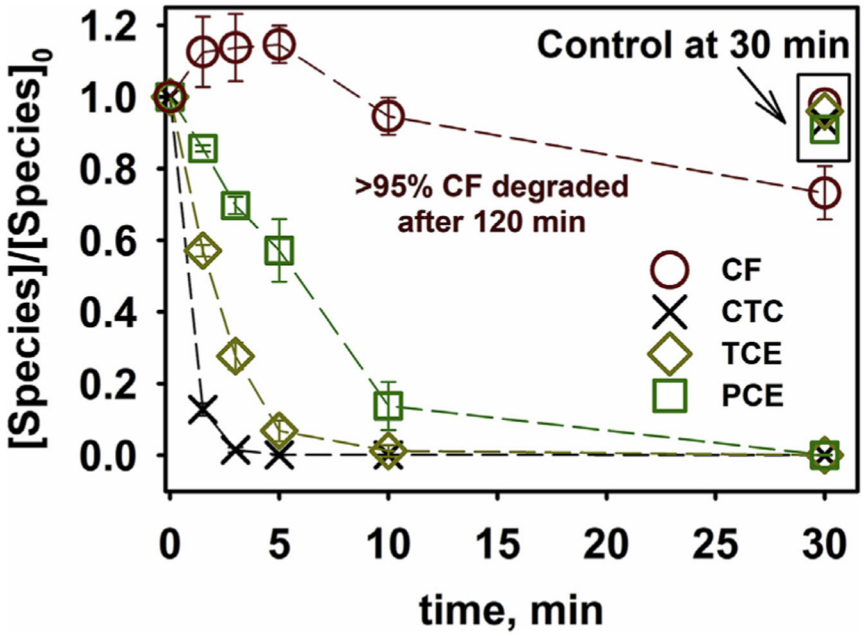

Fig. 8.

Groundwater samples were treated with Pd/Fe nanoparticles in a solution phase study ([Fe] = 72 mg/L, Pd is 0.5 wt% of Fe, 0.5 wt% CMC solution, T = 23 °C, initial pH = 7.8). After post filtration and acid dissolution, the samples were analyzed in purge and trap GC-MS method. The compounds are: chloroform (CF), carbon tetrachloride (CTC), trichloroethylene (TCE) and tetrachloroethylene (PCE). The initial concentration ($[Species]_o$) were directly measured of the groundwater samples with the same filtration and acid dissolution steps. Deliberately oxidized Pd/Fe particles were used as the control groups.

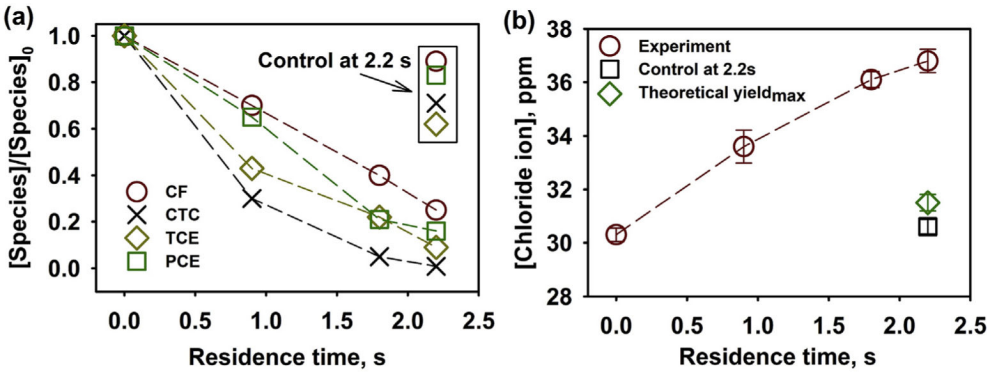

Fig. 9.

Groundwater samples were treated by permeating through the Pd/Fe membrane (12.1 wt% PMAA, permeability at pH 7.8 was tested as 25 LMH/bar, [Fe] = 4.1 mg per membrane, effective external area 11.2 cm^2, Pd is 0.5 wt% of Fe, initial pH = 7.8, T = 23 °C). (a) The $[Species]_0$ results came from direct measurement of the groundwater sample. (b) Corresponding chloride concentration was measured by using a chloride electrode. The theoretical $yield_{max}$ indicates the maximum chloride production of four chlorinated compounds. The compounds are: chloroform (CF), carbon tetrachloride (CTC), trichloroethylene (TCE) and tetrachloroethylene (PCE). Deliberately oxidized Pd/Fe membranes were used as the control groups.

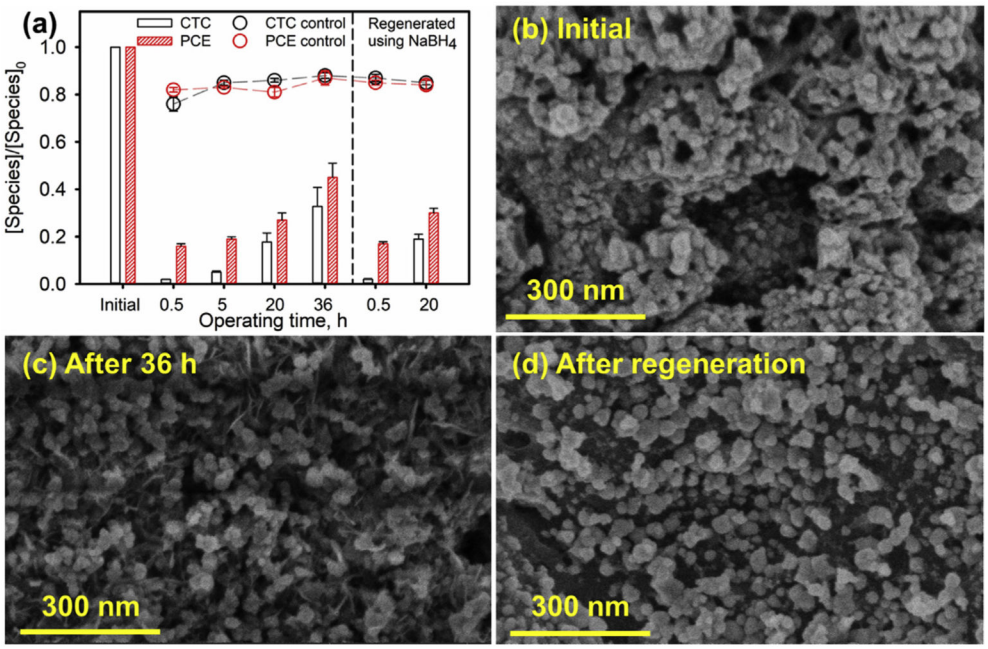

Fig. 10.

The long-term degradation study of the functionalized Pd/Fe-PMAA-PVDF membranes was conducted in convection flow (12.1 wt% PMAA, permeability at pH 7.8: 25 LMH/bar, [Fe] = 4.1 mg per membrane, effective external area 11.2 cm^2, Pd is 0.5 wt% of Fe, initial pH = 7.8, T = 23 °C). Synthetic water was prepared with the similar concentrations of those in the groundwater (35 ppb carbon tetrachloride (CTC) and 950 ppb tetrachloroethylene (PCE)). The deliberately oxidized functionalized membranes were used as the control groups and these membranes were oxidized again after $NaBH_4$ regeneration process. Figure (a): degradation performance in a continuous flow at 0.34 bar (residence time 2.2 s). Figure (b, c, d): the reactive particles on the membrane surface were characterized in three different conditions.

Table 1

Properties of pristine and PMAA functionalized PVDF membranes (1 mol% initiator and 1 mol% cross linker).

PVDF 700	Pore size (nm)	Mass gain (%)	Thickness (μm)	Contact angle (°) at pH 5.5	Permeability (LMH/bar) at pH 2.3	Permeability (LMH/bar) at pH 10.5
Pristine	123.8 ± 78.6	N/A	170.2 ± 4.1	87.5 ± 1.8	6611 ± 55	6589 ± 57
Functionalized	60.6 ± 16.7	12.1	172.4 ± 2.4	54.1 ± 2.3	543 ± 4	18.2 ± 0.5

Table 2

Analysis results of the collected groundwater samples during spring and summer in 2018. Volatile chlorinated species (unit, ppb) were analyzed using purge and trap GC-MS method.

Species	Chloroform (CF)	Carbon tetrachloride (CTC)	Trichloroethylene (TCE)	Tetrachloroethylene (PCE)
Spring samples	32 ± 1	39 ± 1	185 ± 1	980 ± 2
Summer samples	25 ± 1	31 ± 1	168 ± 2	919 ± 2
[a] EPA MCL drinking water	[b] MCLG 70	5	5	5

pH	Iron ppm	Calcium ppm	Magnesium ppm	Chloride ppm	Hardness as CaC03, ppm	Conductivity pS/cm
7.8	< 0.5	102.0	31.5	[c] 30.3	386.3	986

[a] EPA Maximum Contaminant Level (MCL) – The highest level of a contaminant that is allowed in drinking water. Data obtained from National Primary Drinking Water Regulations (EPA 816-F-09-004).

[b] MCL N/A for chloroform. EPA Maximum Contaminant Level Goal (MCLG) – The level of a contaminant in drinking water below which there is no known or expected risk to health. Data obtained from EPA 816-F-09-004.

[c] Chloride results were analyzed using both the chloride electrode (30.3 ppm) and ion chromatography (26.3 ppm).

Table 3

The surface area normalized reaction rates (k_{sa}, $Lm^{-2}min^{-1}$) of each compound in both solution phase and membrane domain studies of groundwater remediation (0.5 wt% Pd in both cases).

Conditions	CF	CTC	TCE	PCE
[a]Solution phase	0.002	0.101	0.034	0.017
[b]Membrane domain	0.006	0.019	0.009	0.008

[a]Evaluated using a pseudo-first-order reaction, $R^2 > 0.96$ for all.

[b]Evaluated using a plug flow reactor model, $R^2 > 0.94$ for all.